



Magnetic Reconnection May Control the Ion-scale Spectral Break of Solar Wind Turbulence

Daniel Vech¹, Alfred Mallet^{2,3}, Kristopher G. Klein^{1,4}, and Justin C. Kasper¹¹Climate and Space Sciences and Engineering, University of Michigan, Ann Arbor, MI 48109, USA; dvech@umich.edu²Space Science Center, University of New Hampshire, Durham, NH 03824, USA³Space Sciences Laboratory, University of California, Berkeley, CA 94720, USA⁴Lunar and Planetary Laboratory, University of Arizona, Tucson, AZ 85719, USA

Received 2018 February 2; revised 2018 February 27; accepted 2018 February 28; published 2018 March 15

Abstract

The power spectral density of magnetic fluctuations in the solar wind exhibits several power-law-like frequency ranges with a well-defined break between approximately 0.1 and 1 Hz in the spacecraft frame. The exact dependence of this break scale on solar wind parameters has been extensively studied but is not yet fully understood. Recent studies have suggested that reconnection may induce a break in the spectrum at a “disruption scale” λ_D , which may be larger than the fundamental ion kinetic scales, producing an unusually steep spectrum just below the break. We present a statistical investigation of the dependence of the break scale on the proton gyroradius ρ_i , ion inertial length d_i , ion sound radius ρ_s , proton–cyclotron resonance scale ρ_c , and disruption scale λ_D as a function of $\beta_{\perp i}$. We find that the steepest spectral indices of the dissipation range occur when β_e is in the range of 0.1–1 and the break scale is only slightly larger than the ion sound scale (a situation occurring 41% of the time at 1 au), in qualitative agreement with the reconnection model. In this range, the break scale shows a remarkably good correlation with λ_D . Our findings suggest that, at least at low β_e , reconnection may play an important role in the development of the dissipation range turbulent cascade and cause unusually steep (steeper than –3) spectral indices.

Key words: magnetic reconnection – plasmas – solar wind – turbulence – waves

1. Introduction

Plasma in the solar wind exhibits a turbulent cascade over a very wide range of scales (Chen 2016). The turbulent power spectrum consists of several power-law-like ranges, in which different physical mechanisms are involved in the transfer of energy to smaller scales. The scaling behavior of the spectral breaks between these power laws, as well as the spectral indices in the different ranges, provide useful ways to test different turbulence models.

In the “inertial range,” between the outer scale L_{\perp} and an “ion kinetic break scale” $\lambda_B \ll L_{\perp}$, the turbulence appears to mainly consist of strongly nonlinear, highly anisotropic (Horbury et al. 2008), Alfvénically polarized (Belcher & Davis 1971) fluctuations propagating up and down the background magnetic field. The power spectrum of magnetic fluctuations in this range is generally close to $E(k_{\perp}) \propto k_{\perp}^{-5/3}$ (e.g., Matthaeus & Goldstein 1982; Chen et al. 2011).

Below the ion kinetic break scale λ_B , in the so-called “dissipation range,” the turbulent spectrum steepens—generally the spectral index is approximately –2.8 or steeper in this range (below λ_B but above a second break or exponential cutoff at electron kinetic scales; Alexandrova et al. 2009; Sahraoui et al. 2010). This steepening of the spectrum has been explained (Schekochihin et al. 2009; Howes et al. 2011; Boldyrev & Perez 2012) by the fact that below the characteristic ion kinetic scales, the dispersion relation of the characteristic fluctuations of the plasma changes. At moderate-to-high ion plasma beta ($\beta_i = 2\mu_0 n_i k_B T_i / B_0^2$), Alfvén waves

(AW) transition into dispersive kinetic Alfvén waves (KAW) when the perpendicular wavenumber becomes comparable to the inverse gyroradius, $k_{\perp} \rho_i \sim 1$, where $\rho_i = v_{th\perp i} / \Omega_i$, the ion’s perpendicular thermal speed is $v_{th\perp i} = \sqrt{2k_B T_{\perp i} / m_i}$ and the ion gyrofrequency is $\Omega_i = ZeB_0 / m_i$. For $\beta_i \ll 1$ (and simultaneously, $\beta_e = 2\mu_0 n_e k_B T_e / B_0^2 \ll 1$), this transition occurs at $k_{\perp} \rho_s \sim 1$, where $\rho_s = \rho_i \sqrt{ZT_e / 2T_i}$ is the ion sound radius. Thus, one might expect $\lambda_B \sim \rho_i$ at $\beta_i \gtrsim 1$ and $\lambda_B \sim \rho_s$ at $\beta_i \ll 1$. The former scaling appears in measurements of the break scale at $\beta_i \sim 1$ (Alexandrova et al. 2009; Sahraoui et al. 2010). However, Chen et al. (2014) studied the behavior of λ_B in two different regimes. For $\beta_i \gg 1$, they found $\lambda_B \sim \rho_i$ as expected from the KAW dispersion relation. On the other hand, for $\beta_i \ll 1$, they found that the break scale was much closer to the ion inertial length, $\lambda_B \sim d_i = c / \omega_{pi} = \rho_i / \sqrt{\beta_i}$ where $\omega_{pi} = \sqrt{n_i Z^2 e^2 / \epsilon_0 m_i}$ is the ion plasma frequency; rather than $\lambda_B \sim \rho_s$ as would be expected from the KAW dispersion relation. Several studies have suggested that the break frequency in the $\beta_i \sim 1$ case can be well approximated with the proton–cyclotron resonance scale defined as $\rho_c = d_i + \sigma_i$ where the pseudo-gyroscale $\sigma_i = v_{th\parallel i} / \Omega_i$ and $v_{th\parallel i}$ is the ion’s parallel thermal speed (e.g., Bruno & Trenchi 2014; Bruno & Telloni 2015; Woodham et al. 2018). This method relies on the cyclotron resonance condition for protons, which is satisfied when k_{\parallel} is large enough to allow resonance with the proton population. Since the turbulence is usually highly anisotropic ($k_{\perp} \gg k_{\parallel}$; e.g., Chen et al. 2010a, 2010b) the measured frequency spectrum generally corresponds to a k_{\perp} wavenumber spectrum and so the proton–cyclotron resonance scale cannot explain the break without also posing an injection of energy into magnetic fluctuations at high k_{\parallel} (e.g., by instabilities, see Klein & Howes 2015).

The β_i -dependent behavior of the ion-scale break is thus somewhat of a mystery. The goal of this Letter is to study the behavior of λ_B across the whole range of $\beta_{\perp i}$ in the solar wind, thus extending the work of Chen et al. (2014) on how λ_B behaves at extreme $\beta_{\perp i}$ values.

Recently, Mallet et al. (2017) and Loureiro & Boldyrev (2017) proposed that sheet-like turbulent structures naturally generated by the inertial range turbulence dynamics (Boldyrev 2006; Chandran et al. 2015; Howes 2016; Mallet et al. 2016; Mallet & Schekochihin 2017; Verdini et al. 2018) may be disrupted by the onset of reconnection below a characteristic “disruption scale,”

$$\lambda_D[n = 2] = C_D L_{\perp}^{1/9} (d_e \rho_s)^{4/9}, \quad (1)$$

where $d_e = c/\omega_{pe}$ is the electron inertial length, $\omega_{pe} = \sqrt{n_e e^2 / \epsilon_0 m_e}$ is the electron plasma frequency and C_D is an undetermined dimensionless prefactor of the order of unity. $\lambda_D[n = 2]$ is the disruption scale of the so-called “ $n = 2$ ” fluctuations, which determine the second-order structure function and power spectrum. Since a detailed study of intermittency (fluctuations with $n \neq 2$) is beyond the scope of this paper, we will adopt Equation (1) as a single disruption scale, henceforth denoted λ_D .

Besides Equation (1), there is an alternative scaling proposed by Loureiro & Boldyrev (2017) that relies on a different tearing profile

$$\lambda_D[n = 2] \sim L_{\perp} (d_e / L_{\perp})^{8/21} (\rho_s / L_{\perp})^{10/21}. \quad (2)$$

The two scalings are observationally indistinguishable from one another in our data set. Due to this close agreement, we elect to use Equation (1) in this Letter.

Equation (1) is only valid when λ_D is larger than the fundamental ion kinetic scale at which the waves become dispersive (i.e., ρ_s), which happens for $\beta_e < \beta_e^{\text{crit}}$ given by

$$\beta_e^{\text{crit}} = C_D^{9/2} \frac{Z m_e}{2 m_i} \left(\frac{L_{\perp}}{\rho_s} \right)^{1/2}, \quad (3)$$

thus, at low β_e , reconnection may induce a break to a steeper spectrum at a larger scale than one might expect solely on the basis of the KAW dispersion relation.

This reconnection model relies on the phenomenon of dynamic alignment, which leads to three-dimensionally (3D) anisotropic eddies and a $-3/2$ spectral index in the inertial range (Boldyrev 2006; Chandran et al. 2015; Mallet & Schekochihin 2017). Although solar wind measurements indicate that the spectral index is closer to $-5/3$, several observational studies have found clear evidence for 3D anisotropy of the turbulence (Chen et al. 2012; Vech & Chen 2016; Verdini et al. 2018), suggesting that one might expect the structure to be unstable to the onset of reconnection at λ_D .

Mallet et al. (2017) suggested that the turbulent fluctuations are converted from sheet-like structures above λ_D to flux-rope-like (or vortex-like) structures just below λ_D —such “Alfvén vortex” structures have been observed in the solar wind just above the ion scales (Alexandrova 2008; Lion et al. 2016; Perrone et al. 2016; Roberts et al. 2016; Perrone et al. 2017), although the exact mechanism generating these structures is a matter of debate. This significantly accelerates the cascade of the disrupted structures. In order to maintain constant energy

flux through scale, the turbulent structures therefore adjust with a sudden drop in amplitude at the disruption scale. The flux-rope-like structures then cascade as is usual in Alfvénic turbulence, becoming progressively more sheet-like, and so on—until the scale at which the KAW dynamics take over, ρ_s . The relatively shallow spectral index associated with the usual Alfvénic dynamics present in this secondary cascade will act to “smooth out” the rapid drop in amplitude associated with disruption events. This smoothing is increasingly effective as the scale separation between λ_D and ρ_s increases; i.e., as the range of scales over which the usual Alfvénic dynamics apply becomes more important relative to the sudden drop in amplitude caused by disruption. Specifically, Mallet et al. (2017) predict that between λ_D and ρ_s , the power spectrum would be steeper than k_{\perp}^{-3} , becoming progressively steeper as $\lambda_D \rightarrow \rho_s$ from above (i.e., the spectrum is predicted to be steepest when β_e is only moderately low, so that λ_D is only slightly larger than ρ_s). Therefore, reconnection may fundamentally change the nature of the small-scale fluctuations.

In this Letter, we use over 13 years of Wind spacecraft data to study the ion spectral break scale λ_B and dissipation-range spectral index, and how these depend on fundamental ion length scales ρ_i , ρ_s , d_i , ρ_c , and the disruption scale λ_D , as well as on the fundamental parameters $\beta_{\perp i}$ and β_e . We will show that, at least in terms of scalings, λ_D from the reconnection model (Mallet et al. 2017) seems to correlate with the measured behavior of the break scale λ_B of the solar wind turbulent power spectrum better than any of the fundamental ion kinetic scales. In addition to this, the steepest spectral indices appear at moderately low β_e , and when λ_B is only slightly larger than ρ_s , as expected qualitatively from the reconnection model. Both of these observations suggest that reconnection may play an important role in the development of the dissipation range turbulent cascade.

2. Method

We use a statistical approach based on Wind spacecraft observations to study the variation of the break scale as a function of physical parameters. The investigated period extends from 2004 January to 2016 December during which Wind was in the pristine solar wind. The time series of the magnetic field (11 Hz; Lepping et al. 1995), on board ion moments, ion parameters (92 s cadence both), and electron moments (37 s cadence; Lin et al. 1995; Ogilvie et al. 1995) were split into 10 minute intervals ($\sim 5.8 \times 10^5$ intervals overall) and the averages of $\beta_{\perp i}$, β_e , d_i , ρ_i , ρ_s , and ρ_c in each interval were calculated.

To estimate λ_D , we use Equation (1), and assume that the break frequency between the energy-containing and inertial ranges is a constant 10^{-4} Hz (Podesta et al. 2007), calculating $L_{\perp} = V_{sw} / (2\pi 10^{-4})$. The average value of L_{\perp} in our study is 7.4×10^5 km, in good agreement with previous studies, which suggest that $L_{\perp} \sim 10^6$ km under average solar wind conditions (Matthaeus et al. 2014). While we do not expect the outer scale to be truly constant over the 13 years of data, in practice this does not introduce a significant source of error in our estimate of λ_D , since it appears only as a nearly constant factor of $L_{\perp}^{1/9}$ in Equation (1). We will determine the dimensionless prefactor C_D in Equation (1) from the data.

For each interval, the power spectral density (PSD) of each magnetic field component was computed via Fourier transform and then the components were summed up to obtain the total

PSD (Koval & Szabo 2013). The spectral index and ion-scale break frequency (f_b) were identified using the approach of Vech et al. (2017). A sequence of 43 logarithmically spaced frequencies was generated from 0.1 to 5.17 Hz and 33 linear fits were made in frequency ranges between the i th and $i + 10$ th elements of this sequence having a ratio of 2.55. From this set of fits, the steepest spectral index was selected and the low frequency end was identified as f_b . The overall distribution of f_b shows excellent agreement with the study of Markovskii et al. (2008), where f_b was identified manually for 454 solar wind intervals. The mean and standard deviation of the dissipation range spectral index is -2.99 ± 0.65 in excellent agreement with previous studies (e.g., Leamon et al. 1998; Smith et al. 2006). We note that we filtered out cases when the dissipation range spectral index and f_b were affected by the noise floor; see Vech et al. (2017).

3. Results

To study the scaling behavior of f_b as a function of physical parameters in Figure 1, we plot 2D histograms of f_b normalized to frequencies corresponding to five scales of interest. In all panels, the data is binned in a 50×50 grid, and bins with fewer than 10 samples are discarded. For each 5% of the data (as binned by the quantity on the x-axis), the averages and standard deviation of the quantity on the y-axis are plotted, together with the best power-law fit to the whole 2D distribution of the raw data. These power-law exponents and their 95% confidence intervals from Figure 1 are summarized in Table 1.

Figures 1(a) and (b) show the ratio of the break frequency and the frequency corresponding to the convected ion gyroradius ($f_{\rho_i} = V_{sw}/(2\pi\rho_i)$) and ion inertial length ($f_{d_i} = V_{sw}/(2\pi d_i)$) as a function of $\beta_{\perp i}$, respectively. Our results agree with Chen et al. (2014): for solar wind intervals with $\beta_{\perp i} \ll 1$ the break closely aligns with f_{d_i} , while in the $\beta_{\perp i} \gg 1$ case the break is closest to f_{ρ_i} ; however, this appears to be a coincidence—the white curves and the 2D histograms show no sign of “flattening” and becoming independent of $\beta_{\perp i}$ at high or low $\beta_{\perp i}$ in Figures 1(a) and (b) respectively. We therefore find little evidence that the behavior of the break is truly explained by either ρ_i at $\beta_{\perp i} \gg 1$ or d_i at $\beta_{\perp i} \ll 1$. Indeed, the white lines in Figure 1 show no significant difference from the overall best-fit power laws shown in black for any value of $\beta_{\perp i}$. Overall, the break frequency shows significantly stronger dependence on f_{ρ_i} than f_{d_i} ; we will discuss one potential reason for the rather shallow dependence of f_b/f_{d_i} at the end of this section.

Figure 1(c) shows the ratio of f_b/f_{ρ_s} ($f_{\rho_s} = V_{sw}/(2\pi\rho_s)$) as a function of $\beta_{\perp i}$, respectively. Similarly to f_b/f_{ρ_i} and f_b/f_{d_i} , f_b/f_{ρ_s} has a clear dependence on $\beta_{\perp i}$. We therefore conclude that neither ρ_i , d_i , nor ρ_s can physically explain the behavior of the ion break scale in the solar wind.

On the other hand, Figure 1(d) shows that f_b/f_{λ_D} ($f_{\lambda_D} = V_{sw}/(2\pi\lambda_D)$) is nearly constant as a function of $\beta_{\perp i}$. This suggests that the ion break scale in the solar wind may be determined by λ_D given by Equation (1), as predicted by the reconnection model of Mallet et al. (2017). One obvious caveat to this is that the value of f_b/f_{λ_D} is significantly less than unity, by around half an order of magnitude, across the whole range of $\beta_{\perp i}$.

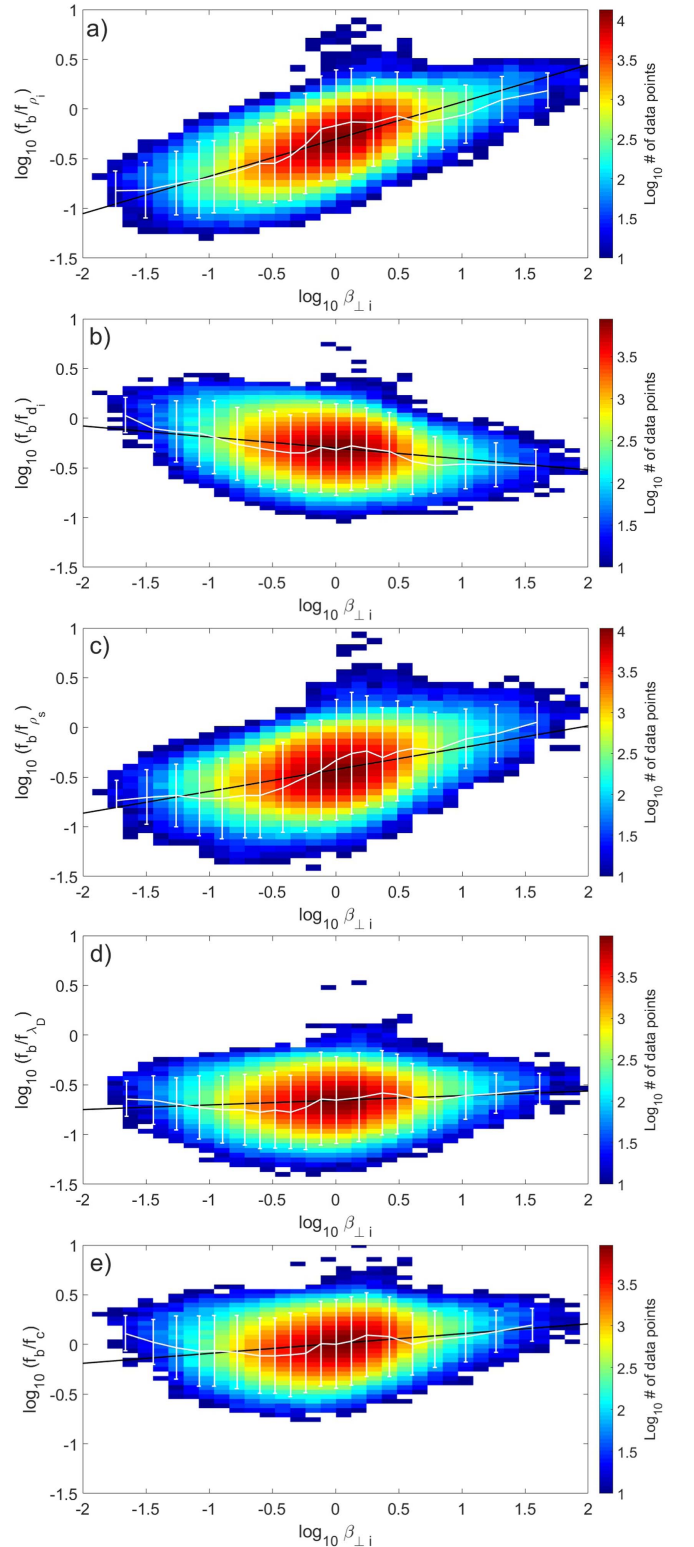


Figure 1. The 2D histograms show the number of data points in each bin in the (a) $(f_b/f_{\rho_i}, \beta_{\perp i})$, (b) $(f_b/f_{d_i}, \beta_{\perp i})$, (c) $(f_b/f_{\rho_s}, \beta_{\perp i})$, (d) $(f_b/f_{\lambda_D}, \beta_{\perp i})$, and (e) $(f_b/f_c, \beta_{\perp i})$ grids, respectively. In each panel, least-square fits are indicated with black lines; their slopes are summarized in Table 1. For each 5% of the data (as binned by the quantity on the x-axis), the averages and standard deviation of the quantity on the y-axis are plotted in white.

In Figure 1(e), the frequency corresponding to the proton-cyclotron resonance scale ($f_c = V_{sw}/(2\pi\rho_c)$) also shows reasonable agreement with the break frequency across the

Table 1
Summary of the Power-law Fits Shown in Figures 1, 3, and 4

Parameters	Slope of the Power-law Fit	95% Confidence Interval
f_b/f_{ρ_i} versus $\beta_{\perp i}$	0.377	[0.376, 0.379]
f_b/f_{d_i} versus $\beta_{\perp i}$	-0.107	[-0.109, -0.106]
f_b/f_{ρ_s} versus $\beta_{\perp i}$	0.219	[0.2183, 0.221]
f_b/f_{λ_D} versus $\beta_{\perp i}$	0.046	[0.0454, 0.0479]
f_b/f_c versus $\beta_{\perp i}$	0.099	[0.0979, 0.1005]
f_b/f_{λ_D} versus $\beta_{\perp i}$	-1.9×10^{-4}	[-0.0020, 0.0016]
f_b/f_c versus $\beta_{\perp i}$	0.1047	[0.1028, 0.1066]
β_i versus T_e/T_p	-0.317	[-0.3200, -0.3156]

entire distribution of $\beta_{\perp i}$: its best-fit slope parameter is only slightly larger than that of f_b/f_{λ_D} (Table 1). Based on these observations alone, we cannot conclusively identify if λ_D or ρ_c controls the break frequency.

In Figure 2, the $(f_b/f_{\rho_s}, \beta_e)$ plane is shown and the color represents the median dissipation range spectral index in each bin. The distribution indicates a significant steepening of the spectral index at “moderately” small β_e values between approximately 0.1–1, where f_b is slightly smaller than f_{ρ_s} . In this region, the spectral indices are typically steeper than -3 in a narrow range just above the break (see Sahraoui et al. 2010). Mallet et al. (2017) predict that the steepest indices should be attained for β_e values just low enough that the reconnection-induced break occurs only just before the transition from AW to KAW (at the ion scale). Our technique (see Section 2) measures the spectral index over a fixed range of $[f_b, 2.55 \cdot f_b]$. If there is a steep subrange narrower than this just above the break, this approach cannot capture its true steepness. Due to this limitation in our fitting technique as well as the narrow range of scales involved, we are only able to claim qualitative similarity with the Mallet et al. (2017) prediction.

To resolve the ambiguous results obtained with Figures 1(d) and (e), we repeat our analysis with the subset of the data within the black square in Figure 2, which encloses 41% of the total data and is bounded by $0.1 \lesssim \beta_e \lesssim 1$ and $0.12 \lesssim f_b/f_{\rho_s} \lesssim 0.63$. The spectral indices are significantly steeper in this region, and if this is caused by reconnection, then λ_B may have significantly better scaling with λ_D in the marked region than with ρ_c . In Figure 3(a), the slope of the power-law fit for f_b/f_c as a function of $\beta_{\perp i}$ closely agrees with the one based on the full distribution. In contrast, in Figure 3(b), the slope of the power-law fit for f_b/f_{λ_D} as a function of $\beta_{\perp i}$ is remarkably close to 0. Based on this, we suggest that at least at low β_e magnetic reconnection may control the ion-scale break of the solar wind turbulence. The intercept of the power-law fit is $10^{-0.6728}$, implying $C_D = 4.7$ (see Equation (1)).

Both f_b/f_{λ_D} and f_b/f_c were close to normally distributed in our data, thus we use an F -test to investigate whether they have equal variance. The ratio of the sample variances is $F = \sigma_{(f_b/f_{\lambda_D})}^2 / \sigma_{(f_b/f_c)}^2 = 0.8398$ with 95% confidence intervals of [0.8328; 0.8468]. Thus we reject the null hypothesis and conclude that λ_D predicts the break with smaller spread than ρ_c .

Finally, the scaling of f_b/f_{d_i} as a function of β_i , while significant over the whole range of β_i present in the data, is not particularly strong. With reference to the results of Chen et al.

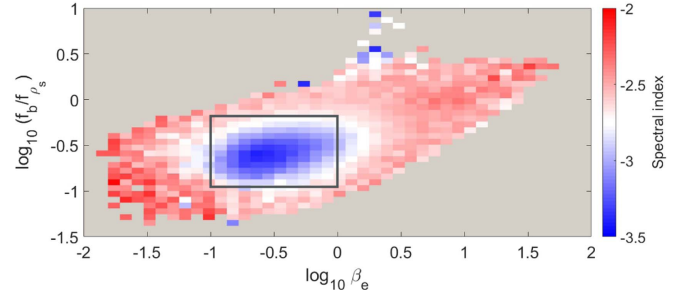


Figure 2. Spectral index of the dissipation range binned in the $(f_b/f_{\rho_s}, \beta_e)$ plane. The black square marks the region with the steepest spectral indices in the range of $0.1 \lesssim \beta_e \lesssim 1$ and $0.12 \lesssim f_b/f_{\rho_s} \lesssim 0.63$.

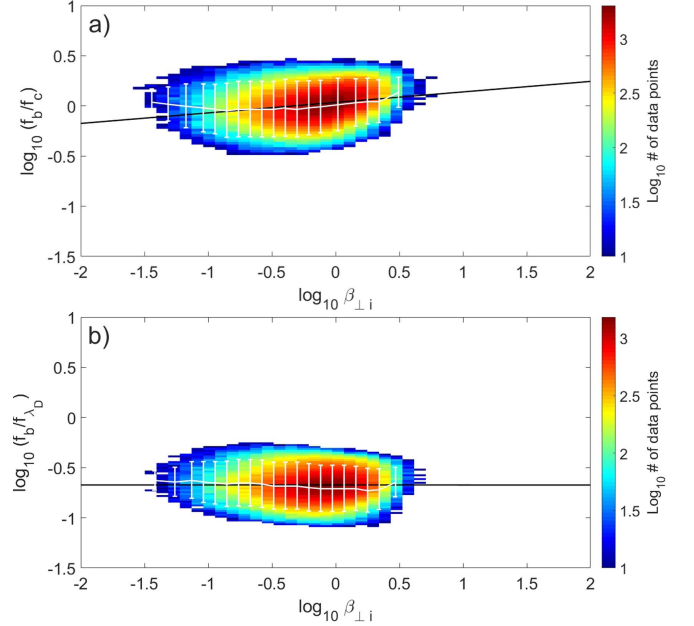


Figure 3. (a) and (b) are identical to Figures 1(e) and (d); however, they present the subset of measurements, which are within the black square in Figure 2 corresponding to 41% of the overall data points.

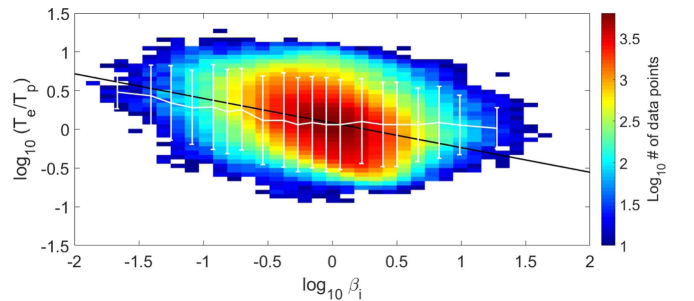


Figure 4. 2D histogram showing the distribution of the measurements in the $(\beta_i, T_e/T_p)$ plane. The least-square fit is indicated with a black line and the average and standard deviation of each 5% of the data are marked in white.

(2014), Mallet et al. (2017) pointed out that correlations between T_e/T_i and β_i could cause the scaling behavior of d_i to mimic that of λ_D . Neglecting a nearly constant factor $(L_{\perp}/\rho_s)^{1/9}$,

$$\frac{\lambda_D}{\rho_s} \propto \beta_e^{-2/9} \Rightarrow \frac{\lambda_D}{d_i} \propto \left(\beta_i \frac{T_e}{T_i} \right)^{5/18}, \quad (4)$$

and so if T_e/T_i were anticorrelated with β_i , the ratio λ_D/d_i would scale less strongly with β_i than otherwise expected.

Figure 4 shows that empirically, such an anticorrelation does in fact exist in the solar wind (at least at low β_i). Assuming that the break scale $\lambda_B \propto \lambda_D$ (as does appear to be the case: see Figures 1(d) and 3(b)), this contributes to the rather shallow scaling of f_b/f_{d_i} in Figure 1(b). Similar consideration could contribute to the shallow scaling of f_b/f_c with $\beta_{\perp i}$.

4. Conclusion

In this Letter, we have presented a statistical study of the break scale λ_B between the inertial and dissipation ranges of the solar wind turbulence spectrum, and to what extent λ_B agrees with the fundamental ion length scales ρ_i , d_i , ρ_s , ρ_c and the disruption scale λ_D (Equation (1)), as a function of $\beta_{\perp i}$. Our results suggest that the ion-scale break of the solar wind turbulence may be controlled by magnetic reconnection in the low β_e (0.1–1) case, which is the main result of this Letter.

The observed behavior of f_b/f_{ρ_i} and f_b/f_{d_i} as a function of $\beta_{\perp i}$ are consistent with previous studies based on more limited data sets (Chen et al. 2014; Wang et al. 2018): for $\beta_{\perp i} \ll 1$ the break occurs at the frequency of f_{d_i} and for $\beta_{\perp i} \gg 1$ the break is closest to f_{ρ_i} . However, both f_b/f_{ρ_i} and f_b/f_{d_i} showed significant dependence on $\beta_{\perp i}$ across the whole range of $\beta_{\perp i}$ present in the data, suggesting that the agreement with the break frequency in narrow ranges at the extremes of $\beta_{\perp i}$ is somewhat coincidental. Thus, we find little evidence that either ρ_i or d_i determine the break in the power spectrum. Similarly, f_b/f_{ρ_c} has a clear scaling with $\beta_{\perp i}$ and thus cannot explain the position of the break.

This contrasts with recent hybrid simulations by Franci et al. (2016), which found that for $\beta_{\perp i} \ll 1$, $\lambda_B \sim d_i$ independently of β_i , and for $\beta_{\perp i} \gg 1$, $\lambda_B \sim \rho_i$ independently of $\beta_{\perp i}$. We note, however, that their simulations may contain different physics than the true solar wind turbulence; they are two-dimensional, and also do not contain the electron inertial scale, which allows the reconnection to occur in the model of Mallet et al. (2017).




Comparing the break scale to the scale predicted by the reconnection model (Loureiro & Boldyrev 2017; Mallet et al. 2017), we found that f_b/f_{λ_D} was nearly independent of $\beta_{\perp i}$. To obtain agreement in the magnitudes of λ_B and λ_D a dimensionless prefactor $C_D = 4.7$ must be inserted into Equation (1) since this cannot be predicted from the simplified model in Mallet et al. (2017), which only predicts scalings. The ratio of the proton–cyclotron resonance scale ρ_c to the break scale showed a similarly shallow scaling with $\beta_{\perp i}$ and the best-fit slope was only a factor of 2.15 steeper than that of f_b/f_{λ_D} . Thus based on the whole distribution of the data we cannot conclusively identify if λ_D or ρ_c controls the break frequency.

At high β_e , reconnection is not expected to cause a break (see Equation (3)); this could be why the agreement between λ_B and λ_D has a slight dependence on $\beta_{\perp i}$ using the whole data set. We therefore repeated our analysis for a significant subset of the data (41% overall) bounded by $0.1 \lesssim \beta_e \lesssim 1$ and $0.12 \lesssim f_b/f_{\rho_c} \lesssim 0.63$ displaying unusually steep spectral indices (steeper than -3), in qualitative agreement with the reconnection model of Mallet et al. (2017). For this subset of the data, we found that λ_B scales with λ_D remarkably well, while $\beta_{\perp i}$ changes two orders of magnitude. In contrast, ρ_c showed a clear correlation with $\beta_{\perp i}$ suggesting that at least at the low β_e case

the break between the inertial and dissipation-range scales may be controlled by the onset of magnetic reconnection.

A. Mallet was supported by NSF grant AGS-1624501. K.G.K. was supported by NASA grant NNX16AM23G. J.C. Kasper was supported by NASA grant NNX14AR78G. Data were sourced from CDAWeb (<http://cdaweb.gsfc.nasa.gov/>).

ORCID iDs

Daniel Vech  <https://orcid.org/0000-0003-1542-1302>
 Kristopher G. Klein  <https://orcid.org/0000-0001-6038-1923>
 Justin C. Kasper  <https://orcid.org/0000-0002-7077-930X>

References

- Alexandrova, O. 2008, *NPGeo*, **15**, 95
 Alexandrova, O., Saur, J., Lacombe, C., et al. 2009, *PRL*, **103**, 165003
 Belcher, J. W., & Davis, L., Jr. 1971, *JGRA*, **76**, 3534
 Boldyrev, S. 2006, *PRL*, **96**, 115002
 Boldyrev, S., & Perez, J. C. 2012, *ApJL*, **758**, L44
 Bruno, R., & Telloni, D. 2015, *ApJL*, **811**, L17
 Bruno, R., & Trenchi, L. 2014, *ApJL*, **787**, L24
 Chandran, B. D. G., Schekochihin, A. A., & Mallet, A. 2015, *ApJ*, **807**, 39
 Chen, C., Horbury, T., Schekochihin, A., et al. 2010a, *PRL*, **104**, 255002
 Chen, C., Wicks, R., Horbury, T., & Schekochihin, A. 2010b, *ApJL*, **711**, L79
 Chen, C. H. K. 2016, *JPP*, **82**, 535820602
 Chen, C. H. K., Leung, L., Boldyrev, S., Maruca, B. A., & Bale, S. D. 2014, *GRL*, **41**, 8081
 Chen, C. H. K., Mallet, A., Schekochihin, A. A., et al. 2012, *ApJ*, **758**, 120
 Chen, C. H. K., Mallet, A., Yousef, T. A., Schekochihin, A. A., & Horbury, T. S. 2011, *MNRAS*, **415**, 3219
 Franci, L., Landi, S., Matteini, L., Verdini, A., & Hellinger, P. 2016, *ApJ*, **833**, 91
 Horbury, T. S., Forman, M., & Oughton, S. 2008, *PRL*, **101**, 175005
 Howes, G. G. 2016, *ApJL*, **827**, L28
 Howes, G. G., Tenbarge, J. M., Dorland, W., et al. 2011, *PRL*, **107**, 035004
 Klein, K. G., & Howes, G. G. 2015, *PhPI*, **22**, 032903
 Koval, A., & Szabo, A. 2013, in AIP Conf. Proc. 1539, SOLAR WIND 13: Proceedings of the Thirteenth International Solar Wind Conference, ed. G. P. Zank et al. (Melville, NY: AIP), 211
 Leamon, R. J., Smith, C. W., Ness, N. F., Matthaeus, W. H., & Wong, H. K. 1998, *JGRA*, **103**, 4775
 Lepping, R., Acuña, M., Burlaga, L., et al. 1995, *SSRv*, **71**, 207
 Lin, R., Anderson, K., Ashford, S., et al. 1995, *SSRv*, **71**, 125
 Lion, S., Alexandrova, O., & Zaslavsky, A. 2016, *ApJ*, **824**, 47
 Loureiro, N. F., & Boldyrev, S. 2017, *ApJ*, **850**, 182
 Mallet, A., & Schekochihin, A. A. 2017, *MNRAS*, **466**, 3918
 Mallet, A., Schekochihin, A. A., Chandran, B. D. G., et al. 2016, *MNRAS*, **459**, 2130
 Mallet, A., Schekochihin, A. A., & Chandran, B. D. G. 2017, *JPP*, **83**, 905830609
 Markovskii, S., Vasquez, B. J., & Smith, C. W. 2008, *ApJ*, **675**, 1576
 Matthaeus, W. H., & Goldstein, M. L. 1982, *JGRA*, **87**, 6011
 Matthaeus, W. H., Oughton, S., Osman, K. T., et al. 2014, *ApJ*, **790**, 155
 Ogilvie, K., Chornay, D., Fritzenreiter, R., et al. 1995, *SSRv*, **71**, 55
 Perrone, D., Alexandrova, O., Mangeney, A., et al. 2016, *ApJ*, **826**, 196
 Perrone, D., Alexandrova, O., Roberts, O., et al. 2017, *ApJ*, **849**, 49
 Podesta, J., Roberts, D., & Goldstein, M. 2007, *ApJ*, **664**, 543
 Roberts, O. W., Li, X., Alexandrova, O., & Li, B. 2016, *JGRA*, **121**, 3870
 Sahaoui, F., Goldstein, M. L., Belmont, G., Canu, P., & Rezeau, L. 2010, *PRL*, **105**, 131101
 Schekochihin, A. A., Cowley, S. C., Dorland, W., et al. 2009, *ApJS*, **182**, 310
 Smith, C. W., Hamilton, K., Vasquez, B. J., & Leamon, R. J. 2006, *ApJL*, **645**, L85
 Vech, D., & Chen, C. H. 2016, *ApJL*, **832**, L16
 Vech, D., Klein, K. G., & Kasper, J. C. 2017, *ApJL*, **850**, L11
 Verdini, A., Grappin, R., Alexandrova, O., & Lion, S. 2018, *ApJ*, **853**, 85
 Wang, X., Tu, C.-Y., He, J.-S., & Wang, L.-H. 2018, *JGRA*, **123**, 68
 Woodham, L. D., Wicks, R. T., Verscharen, D., & Owen, C. J. 2018, arXiv:1801.07344